JACS
JOURNAL OF THE AMERICAN CHEMICAL SOCIETY

Article

pubs.acs.org/JACS

para-Azaquinodimethane: A Compact Quinodimethane Variant as an Ambient Stable Building Block for High-Performance Low Band Gap Polymers

Xuncheng Liu,[†,⊥,#] Bo He,[*,†,#] Christopher L. Anderson,[†,∥] Jun Kang,[‡] Teresa Chen,[†] Jinxiang Chen,[⊥] Shizhen Feng,[⊥] Lianjie Zhang,[⊥] Matthew A. Kolaczkowski,[†,∥] Simon J. Teat,[§] Michael A. Brady,[†,§] Chenhui Zhu,[§] Lin-Wang Wang,[‡] Junwu Chen,[*,⊥] and Yi Liu[*,†,‡]

[†]The Molecular Foundry, [‡]Materials Sciences Division and [§]Advanced Light Source, Lawrence Berkeley National Laboratory, One Cyclotron Road, Berkeley, California 94720, United States

[⊥]Institute of Polymer Optoelectronic Materials & Devices, State Key Laboratory of Luminescent Materials & Devices, South China University of Technology, Guangzhou 510640, P.R. China

[∥]Department of Chemistry, University of California, Berkeley, Berkeley, California 94720, United States

Supporting Information

ABSTRACT: Quinoidal structures incorporating expanded *para*-quinodimethane (*p*-QM) units have garnered great interest as functional organic electronic, optical, and magnetic materials. The direct use of the compact *p*-QM unit as an electronic building block, however, has been inhibited by the high reactivity conveyed by its biradical character. Herein, we introduce a stable *p*-QM variant, namely *p*-azaquinodimethane (*p*-AQM), that incorporates nitrogen atoms in the central ring and alkoxy substituents on the periphery to increase the stability of the quinoidal structure. The succinct synthesis from readily available precursors leads to regio- and stereospecific *p*-AQMs that can be readily integrated into the backbone of conjugated polymers. The quinoidal character of the *p*-AQM unit endows the resulting polymers with narrow band gaps and high carrier transport mobilities. The study of a series of copolymers employing different numbers of thiophene units revealed an unconventional trend in band gaps, which is distinct from the widely adopted donor−acceptor approach to tuning the band gaps of conjugated polymers. Theoretical calculations have shed light on the nature of this trend, which may provide a unique class of conjugated polymers with promising optical and electronic properties.

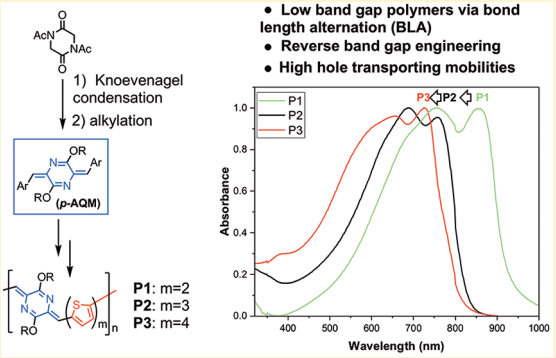

INTRODUCTION

para-Quinodimethane (*p*-QM) is a highly reactive species with a large open-shell biradical character that arises from the drive to recover aromaticity in the biradical benzenoid structure (Scheme 1a).[1] The unique optical and electronic properties associated with both the open-shell and the conjugated closed-shell structures have generated substantial interest due to their potential use in organic electronics and polymer sciences. One notable application of *p*-QMs in materials science that relies on its reactive radical properties is its use in the synthesis of polyphenylenevinylenes (PPVs).[2] A more succinct route to conjugated polymers is to directly incorporate *p*-QM units in the polymer backbone by taking advantage of the conjugation pathway intrinsic in its closed shell form (Scheme 1a). This is, however, highly dependent on the relative stability between the closed and open shell forms. Attempts have been made to strike a balance between the two by incorporating *p*-QMs in extended π-systems or by installation of electron withdrawing groups;[1b,3] however, the use of nonfused *p*-QMs in conjugated polymers remains unexplored.

Another important consideration when employing quinodimethanes in conjugated polymers is their ability to reduce the band gaps of the resulting polymers. Two rational strategies have been established for tuning the band gaps of conjugated polymers:[4] the donor−acceptor approach, in which electron-rich and -deficient units alternate in the polymer backbone,[5] and minimization of bond length alternation (BLA) using quinoidal structures.[3c,6] The donor−acceptor approach has received the majority of the attention in recent literature due to the modular nature of the synthesis of these polymers and the predictable band gap tuning.[7] The latter strategy for the lowering of band gaps, however, deserves attention as a complementary pathway, which operates via a different mechanism and can offer access to frontier energy levels not limited by particular electron donors

Received: April 21, 2017
Published: May 24, 2017

DOI: 10.1021/jacs.7b04031
J. Am. Chem. Soc. XXXX, XXX, XXX−XXX

Scheme 1. (a) Illustration of Resonating *p*-QM Structures as Possible Precursors for Conjugated Polymers, (b) Stable *p*-AQM Reported in This Work, (c) Illustration of BLA Minimization in Low Band Gap Polymers Due to Resonance between Aromatic and Quinoidal Thiophenes, and (d) Low Band Gap *p*-AQM Polymers Highlighting the Resonating Structures between Aromatic and Quinoidal Units

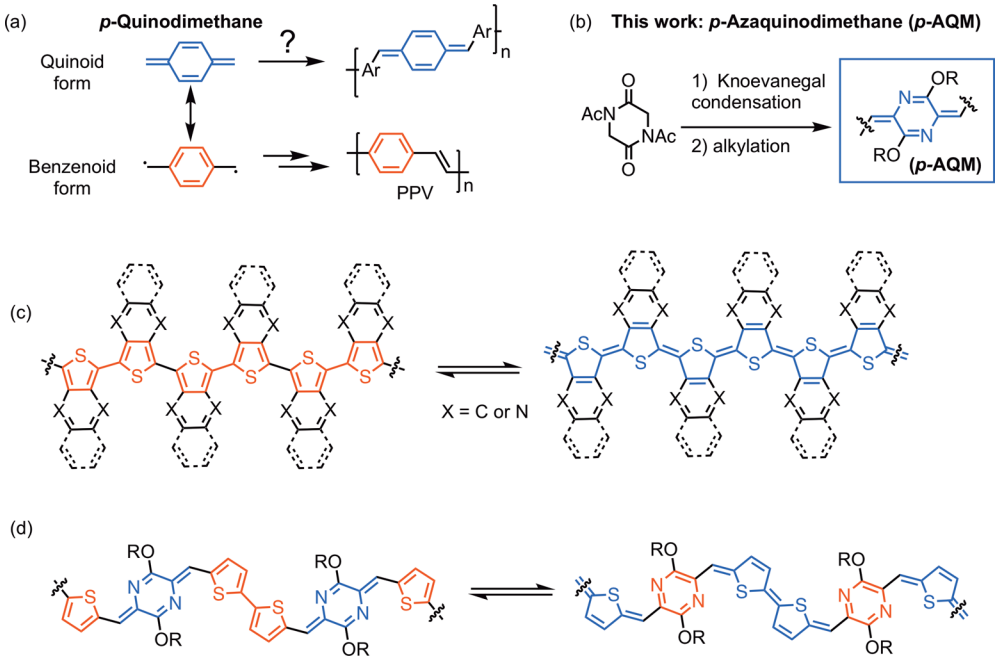

Scheme 2. Synthesis of Substituted *p*-AQMs

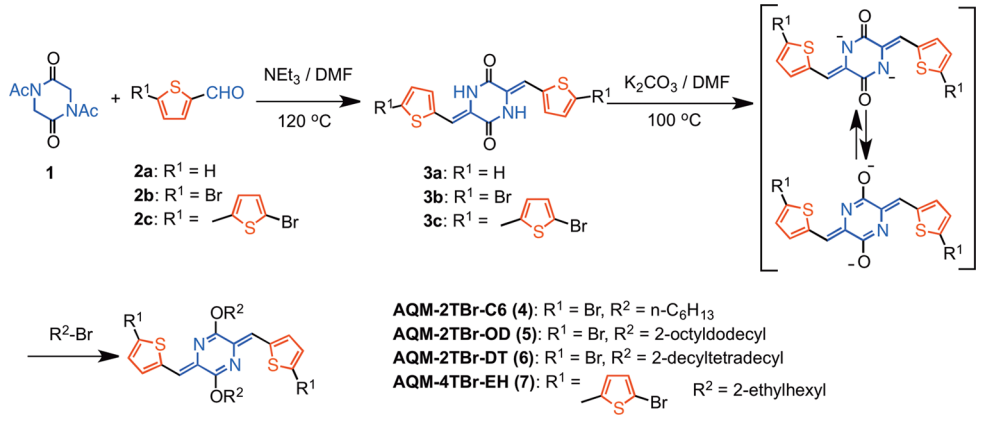

and acceptors. The minimization of BLA in a conjugated system is realized by engendering smaller energy gaps between the aromatic and quinoidal forms of the polymer. In polythiophene, the relatively large band gap correlates with the small contribution of the energetically unfavorable quinoidal structure to the ground state structure of the polymer, which leads to pronounced single bond character in the thiophene-thiophene linkages. The introduction of a quinoidal unit in the backbone chain, such as isothianaphthalene,[8] isonaphthothiophene,[9] thieno[3,4-*b*]pyrazines,[10] and thieno[3,4-*b*]quinoxaline,[10a] where thiophene is fused to an *ortho*-quinodimethane (*o*-QM) moiety, can serve to stabilize the quinoidal form of the neighboring thiophene units (Scheme 1c). In the quinoidal resonance form of the thiophene units, the loss of aromaticity is compensated for by the gain of aromaticity in the fused aromatic rings. The BLAs are correspondingly reduced, giving rise to lower band gaps. In addition to *o*-QMs, the design and incorporation of the *p*-QM structural motif in conjugated polymers has been implemented in a few expanded quinoidal systems,[11] which feature a *p*-benzoquinodimethane core and directly coupled electron-withdrawing carbonyl termini, such as benzodipyrrolidone[12] and benzo[1,2-b:4,5-b′]-dithiophene-2,6-dione.[13] These extended *p*-QM units are sufficiently stable to be employed as effective building blocks for low band gap polymers. However, they are all coupled with electron-withdrawing carbonyl termini, which significantly lower the energy levels of the lowest occupied molecular orbital (LUMO) and thus obscure the boundary between a pure *p*-QM building block and a conventional electron acceptor.

In addition to the approach of introducing electron-withdrawing groups to stabilize π-extended *p*-QMs, heteroatoms could be introduced into the quinoidal skeleton to confer stability.[14] This approach can potentially result in compact *p*-QM cores without expanding the aromatic ring systems, yet a reliable and practical synthesis has never been demonstrated. Here, we show that stable *p*-azaquinodimethane (*p*-AQM) units, in the

DOI: 10.1021/jacs.7b04031
J. Am. Chem. Soc. XXXX, XXX, XXX−XXX

Scheme 3. Synthesis of AQM-Containing Polymers P1−P3

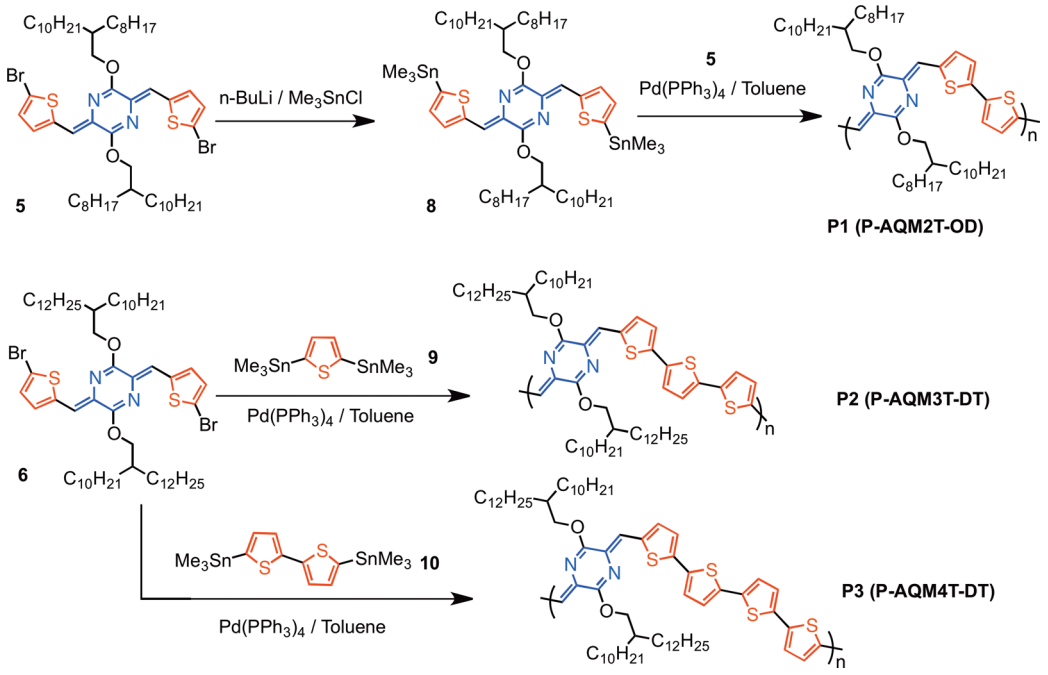

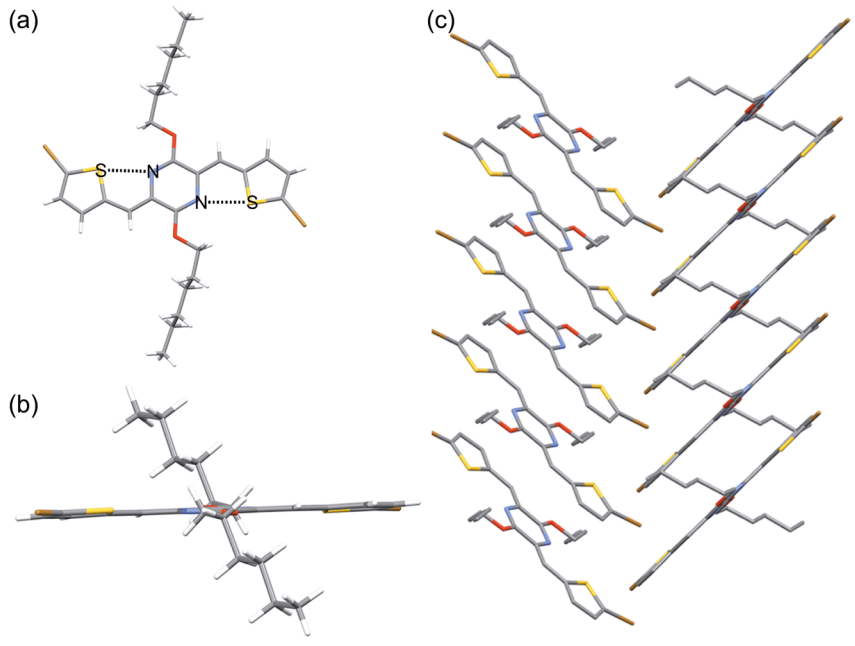

Figure 1. X-ray structures of **4**. Capped stick representation of (a) front view, (b) side view, and (c) herringbone stacking in the solid state. Hydrogen atoms are omitted in (c) for clarity.

form of diarylidene-dialkoxydihydropyrazines, can be prepared via a very succinct synthesis (Scheme 1b). Thanks to the ability of *p*-AQMs to stabilize the quinoidal character of the thiophene comonomers (Scheme 1d), the copolymers of *p*-AQM and oligothiophenes feature low band gaps as well as low LUMO and high HOMO energy levels. We have additionally demonstrated that, in a series of conjugated polymers, the optical band gaps increase with the number of thiophenes in the repeating unit, which stands in contrast to conventional donor−acceptor polymers but is consistent with the expected outcome from BLA minimization in quinoidal-aromatic resonating systems and verified by theoretical calculations. In addition, these AQM-based low band gap polymers exhibit high hole transporting mobilities, which correlate well with their thin film morphologies. The combination of facile synthetic accessibility, high chemical stability, small optical band gaps, tunable optoelectronic properties, and good electronic performance makes *p*-AQM and its derivatives attractive building blocks for use in organic electronics.

RESULTS AND DISCUSSION

Synthesis of *p*-AQMs. Synthesis of *p*-AQMs is furnished in two steps from the readily accessible 1,4-diacetyl-2,5-diketopiperazine (**1**), the cyclic dipeptide skeleton of which is abundant

DOI: 10.1021/jacs.7b04031
J. Am. Chem. Soc. XXXX, XXX, XXX−XXX

in natural products.[15] Knoevenagel condensation between **1** and substituted 2-formylthiophenes (**2a**–**c**) is accompanied by in situ cleavage of the acetyl groups to afford diarylidene piperazinediones in high yields with both alkene groups in the *Z*-configuration (Scheme 2).[16] The subsequent alkylation under mildly basic conditions gives rise exclusively to the *O*-alkylated *p*-AQM products in good to excellent yields. The absence of any *N*-alkylation product suggests that a tautomerization occurs upon deprotonation of the amide.[17] The ambidentate reactivity of amides has also been observed in other polycyclic aromatic amide systems,[18] the ratio of which may be governed by factors such as the choice of base, alkylating reagent, and thermodynamic stability of the final product. This synthesis can be easily carried out on a gram scale and is quite modular, giving rise to a range of *p*-AQMs bearing different aromatic and alkyl groups. Unlike the original *p*-QM, these *p*-AQMs are inert under ambient conditions, can be stored for months without any signs of degradation, and are compatible with the reaction conditions of lithium-halide exchange and metal-catalyzed cross-coupling. As shown in Scheme 3, treating *p*-AQM **5** with *n*-BuLi and Me_3SnCl gives the corresponding bisstannate **8** in 95% yield. Pd-catalyzed cross-coupling polymerization between **5** and **8** affords the corresponding polymer **P1** that contains a *p*-AQM-bithiophene (AQM-2T) repeating unit. **P2** and **P3**, containing a *p*-AQM-terthiophene (AQM-3T) and *p*-AQM-quaterthiophene (AQM-4T) repeating unit, respectively, can be obtained following similar copolymerization procedures. Longer branched side chains are used in **P3** and **P4** to ensure good solubility.

Structural Characterization. The ^1H and ^{13}C NMR spectra are consistent with the *O*-alkylated azaquinodimethane core in structures **4**–**7** (see Supporting Information, SI). Additionally, single-crystal X-ray analyses of **4** and **7** provide unambiguous evidence for the formation of the *p*-AQM core. In the crystal structure of **4**, two crystallographically independent half molecules are present in one unit cell (Figure 1); the bond lengths and connectivity of which are consistent with the *O*-alkylated *p*-AQM structure. In comparing the single crystal structures of **4** and diketopiperazine precursor **3a** (see Figure S1), it can be seen that the arylidene units adopt the *Z*-configuration in both the alkylated *p*-AQM and the precursor. Additionally, the thiophene groups are rotated by 180° after alkylation to favor intramolecular S···N interactions between the thiophene and the *p*-AQM groups. The nitrogen-to-sulfur contact distances of 2.800(3) Å are significantly shorter than the sum of the van der Waals radii of nitrogen and sulfur atoms (3.35 Å), indicating a stabilizing sulfur lone-pair interaction.[19] Such S···N interactions enforce a nearly coplanar thiophene-AQM geometry with a very small dihedral angle of 3.0° between the thiophene and AQM groups. The two crystallographically independent AQM-2T molecules stack into separate 1D columns with an interplane spacing of 3.32 Å and a centroid-to-centroid distance of 4.95 Å between two adjacent *p*-AQMs, which correspond to a slipped π–π stacking and herringbone intercolumnar arrangement. The coplanar conformation and S···N interactions are also observed in the crystal structure of **7** (Figure S1), confirming the generality of such interactions in retaining a flat molecular geometry.

Optical and Optoelectronic Properties. The solution absorption spectrum of **4** (AQM-2T) displays an absorption maximum at 488 nm, which can be ascribed to a π–π^* transition (Figure 2 and Table 1). The absorption maximum is red-shifted to 547 nm in **7** (AQM-4T), which is consistent with the better delocalization of π-electrons along the extended conjugated

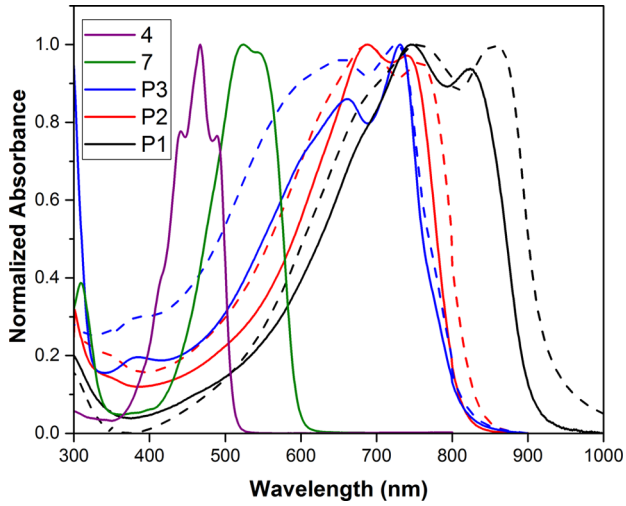

Figure 2. Solution (in chlorobenzene, solid lines) and thin film (dashed lines) absorption spectra of **P1**–**P3**. Solution absorption spectra of **4** and **7** are included for comparison.

system. In the case of polymers, the solution absorption spectrum of **P1** exhibits a narrower bandgap with an absorption maximum and edge at 823 and 903 nm, respectively. A bathochromic shift of ~40 nm is observed between a solution of **P1** and the spuncast thin film, suggesting increased interchain aggregation in the solid state. The optical band gap is estimated to be 1.32 eV from the thin film absorption.

A comparison of the optical band gaps of these *p*-AQM derivatives against conventional donor–acceptor–donor triads and donor–acceptor polymers reveals some noteworthy trends. The lowest-energy optical transition of **4** (AQM-2T) is situated at a considerably shorter wavelength than that of the thiophene-flanked acceptors such as nathphalene diimide (NDI) (NDI-2T, λ = 514 nm),[20] diketopyrrolopyrrole (DPP) (DPP-2T, λ = 548 nm),[21] isoindigo (iID) (iID-2T, λ = 549 nm),[22] bay-annulated indigo (BAI) (BAI-2T, λ = 579 nm)[23] and is similar to benzothiadiazole (BTD) (BTD-2T, λ = 460 nm).[24] On the basis of the absorption properties, *p*-AQM would be expected to be an electron acceptor weaker than NDI, DPP, iID, and BAI and comparable to the medium acceptor BTD. However, the band gap of the AQM-2T-based polymer **P1** is remarkably lower than would be expected from a donor–acceptor polymer containing a medium-strength acceptor and bithiophene donor. As shown in Figure 3, the band gap of **P1** is significantly narrower than these based on a range of electron acceptors with varying strengths, such as NDI,[25] iID,[26] and difluorobenzotriazole (FBTA).[27] Such a contrast suggests that *p*-AQM does not behave like a conventional electron acceptor.

More deviation from common donor–acceptor behavior lies in the trend of the optical band gaps of polymers **P1**–**P3**, which follow the order **P1** < **P2** < **P3**, i.e., the band gap increases with increasing numbers of thiophene units in the conjugated polymer. This trend is the opposite of that observed in conventional donor–acceptor polymers, such as the NDI-nT,[25] iID-nT,[26] and FBTA-nT[27a] examples plotted in Figure 3. Collectively, the incorporation of the *p*-AQM structure into conjugated polymers results in semiconductors with reduced band gaps, yet *p*-AQM behaves distinctively different from that of conventional electron acceptors.

Frontier orbital energy levels of the polymers and small molecules were estimated by cyclic voltammetry using a

DOI: 10.1021/jacs.7b04031
J. Am. Chem. Soc. XXXX, XXX, XXX–XXX

Table 1. Summary of the Optical and Electrochemical Properties and Frontier Orbital Energies

	UV−vis							cyclic voltammetry[b]	
	solution[a]			film					
compd	λ_{max} (nm)	λ_{onset} (nm)	E_g^{opt} (eV)	λ_{max} (nm)	ε[c] (cm^{-1})	λ_{onset} (nm)	E_g^{opt} (eV)	HOMO[d] (eV)	LUMO[e] (eV)
4	488	510	2.43	513	n.m.[f]	576	2.15	−5.06	−2.91
7	547	598	2.07	622	n.m.[f]	710	1.75	−4.85	−3.10
P1	823	903	1.37	855	9.5×10^4	938	1.32	−4.90	−3.58
P2	742	810	1.53	758	5.2×10^4	832	1.49	−5.02	−3.53
P3	731	805	1.54	731	8.5×10^4	810	1.53	−5.07	−3.54

[a]Measured in chlorobenzene. [b]Measured in $CHCl_3$ using a conventional three-electrode setup at a scan rate of 100 mV S^{-1}. [c]Extinction coefficient of thin films. [d]Calculated using $E_{HOMO} = -(4.8 + E_{ox})$ eV. [e]Calculated using the corresponding HOMO level and E_g^{opt}. [f]Not measured.

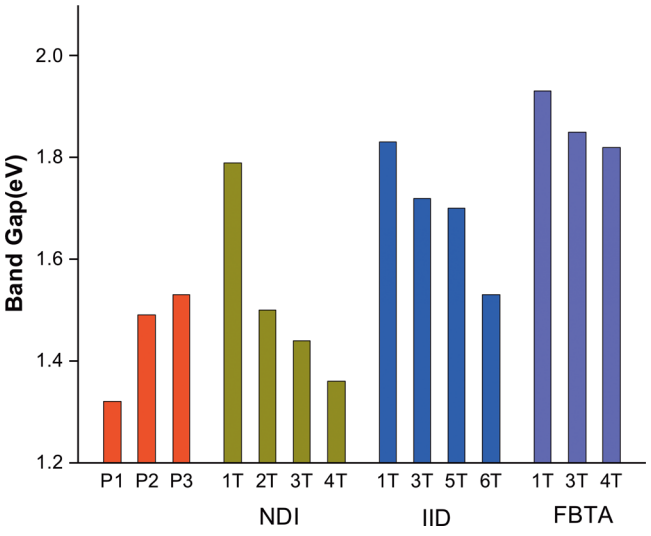

Figure 3. Comparison showing the trends of band gap changes with respect to the numbers of thiophenes in **P1**−**P3** and donor−acceptor polymers based on NDI-*n*T, iID-*n*T, and FBTA-*n*T repeating units, where *n*T refers to the number of thiophenes in the repeating unit.

conventional three-electrode setup and the Fc/Fc^+ redox couple as the internal reference (Figure S2). The LUMO levels of monomeric **4** and polymer **P1** are around −2.9 and −3.6 eV, and the HOMO levels are −5.1 and −4.9 eV, respectively. The high-lying LUMO in **4** confirms the weak electron accepting nature of *p*-AQM. In contrast, the LUMO level is significantly lower in **P1**, which is consistent with very effective orbital delocalization in conjugated polymers. The energy levels of **P2** and **P3** show comparable levels of LUMO energy and a slight decrease in HOMO energy with longer oligothiophene units, commensurate with the observed increasing optical band gaps.

Theoretical Modeling. To understand the trend in band gaps among the polymers **P1**−**P3**, we carried out theoretical modeling to calculate the band structures in the polymers and their small molecule counterparts. The calculations were performed using the Vienna ab initio simulation package (VASP)[28] with the plane-wave projector-augmented wave (PAW) method[29] (see SI for details of modeling). The B3LYP functional[30] was used to describe the exchange-correlation interaction. In all of the models, the longer alkoxy chains are replaced by methoxy groups to reduce computational cost. The influence of the S···N interactions on the preferred conformation was first assessed by comparing the two planar conformations of the AQM-2T polymer where the S atoms in thiophenes are situated close to (conformation 1) or away from (conformation 2) the N atoms in the *p*-AQM ring (Figure 4). The energy of conformation 1 is 0.18 eV/unit cell lower than that of conformation 2, which is consistent with the stabilizing effect brought about by the S···N interactions as observed in single crystals. Conformation 1 is thus adopted in constructing the backbone of all the polymer models. The computed band gap of polymers **P1**−**P3** increases from 1.31 eV for **P1** to 1.50 eV for **P2** to 1.57 eV for **P3**. As the number of thiophene units increases in the monomer, the LUMO increases and the HOMO decreases simultaneously, giving rise to enlarged band gaps (Figure 4). The modeled band gaps are in close agreement with the experimental results. The plots of frontier orbitals indicate that the HOMO and LUMO orbitals are well spread on both the oligothiophene and *p*-AQM units, which differs from the common donor−acceptor scenario where HOMO and LUMO are more localized on individual donor and/or acceptor units.

The increased band gaps from **P1** to **P3** hint of a "dilution effect" wherein the addition of more thiophene units favors the localization of quinoidal character on the *p*-AQM unit and aromatic character on the oligothiophene units. This is indeed supported by comparing the C−C and C═C bond lengths of the oligothiophene segments in the polymers obtained by calculations. Figure 5 shows the carbon−carbon bond length for each bond in the 2T, 3T, and 4T segments. The central thiophene units in 3T and 4T evidently have larger bond length variation than the thiophene units that are directly connected to *p*-AQM units with significantly longer C−C and shorter C═C lengths. These results reveal lessened quinoidal character in the thiophenes that are more distant from the *p*-AQM along the polymer chain, which is consistent with the fact that increasing the number of thiophene units in the polymer chain reduces the resonance contribution from the *p*-AQM unit. It is worth noting that the trend observed in polymers **P1**−**P3** should not be confused with that of the small molecules. The calculated band gaps for small molecules AQM-*n*T ($n = 2$ to 4) follow the order of AQM-2T > AQM-3T > AQM-4T. The HOMO energy level increases and LUMO energy level decreases as the number of thiophene units increases, giving rise to narrower band gaps (Figure S3). Such trends are the opposite of those in the polymers and are also in good agreement with the experimental band gaps of **4** (AQM-2T) and **7** (AQM-4T) (AQM-3T was not synthesized).

Thin Film FETs and Morphologies. Charge transport properties of polymers **P1**−**P3** were evaluated in thin film field effect transistors using the bottom gate/top contact OFET configuration with octadecyltrichlorosilane (OTS)-modified SiO_2 as the dielectric layer. Gold (Au) was used as the source/drain electrodes, and scratched *n*-doped Si was used as the gate electrode. The devices were fabricated using as-cast thin films or those thermally annealed at different temperatures. All the

DOI: 10.1021/jacs.7b04031
J. Am. Chem. Soc. XXXX, XXX, XXX−XXX

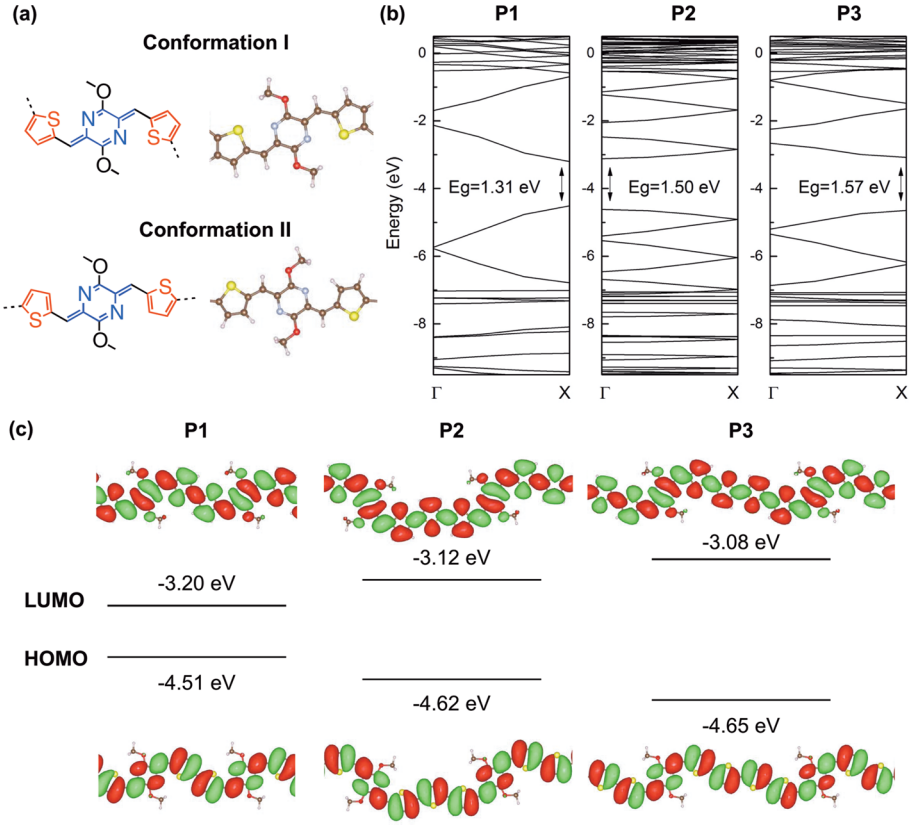

Figure 4. (a) Illustration of the two different conformations of the AQM-2T monomer. (b) Simulated band gaps of **P1**−**P3**. (c) Frontier orbital plots and energy levels of polymers **P1**−**P3**.

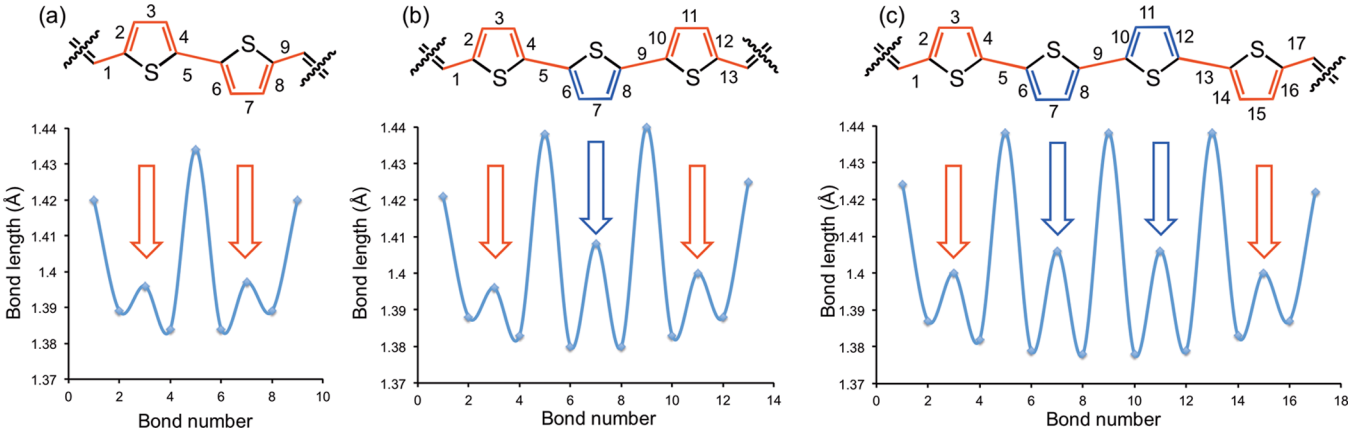

Figure 5. Plots of carbon−carbon bond length for each respective bond number in the oligothiophene units in (a) **P1**, (b) **P2** and (c) **P3**. The red and blue arrows highlight the different thiophene units possessing contrasting BLA characters.

devices displayed distinct *p*-type transporting behavior with output and transfer characteristics summarized in Figure 6, Figure S4, and Table 2. **P2** displayed the best mobility (μ) among all three polymers with the maximum and average reaching 0.54 and 0.47 $cm^2\ V^{-1}\ s^{-1}$, respectively. The average mobilities of **P1** and **P3** are 0.024 and 0.082 $cm^2\ V^{-1}\ s^{-1}$, respectively, which are approximately 20- and 6-times lower than that of **P2**. It should be noted that these mobilties are based on thermally annealed thin films, whereas these as-cast thin films show similar mobilities in the range between 0.01 and 0.02 $cm^2\ V^{-1}\ s^{-1}$. Clearly, the transport properties of these polymers respond very differently to thermal treatment. The mobilities of thermally treated **P1** remains similar to those of the as-cast films, whereas **P2** and **P3** show more than 1 order of magnitude enhancements in average mobility after annealing. Devices fabricated from **P1** after storage for over one year or from **P2** in air show very comparable performances to their respect control devices, suggesting high stability of these AQM-based materials.

Grazing-incidence wide-angle X-ray scattering (GIWAXS) measurements were conducted to probe molecular packing within the spuncast polymer films. For the as-cast thin film of **P1**, strong (001) and (010) scattering peaks are observed in the in-plane and out-of-plane directions, respectively, indicating preferential face-on orientation of the polymer chains on the substrate (Figure 7a). The (010) scattering peak corresponds to π−π stacking between polymer chains with a *d* spacing of 0.39

DOI: 10.1021/jacs.7b04031
J. Am. Chem. Soc. XXXX, XXX, XXX−XXX

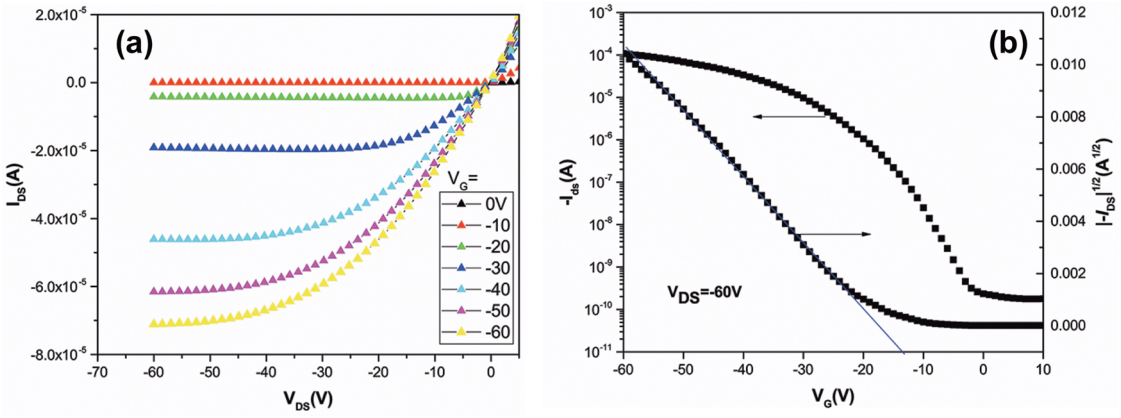

Figure 6. Typical (a) output and (b) transfer characteristics of OFETs based on **P2**.

Table 2. Summary of OFET Characteristics of Polymers P1−P3

compd	film deposition	$\mu_h^{avg,a}$ ($cm^2\ V^{-1}\ s^{-1}$)	μ_h^{dev} ($cm^2\ V^{-1}\ s^{-1}$)	$\mu_h^{max,b}$ ($cm^2\ V^{-1}\ s^{-1}$)	V_{th} (V)	I_{On}/I_{Off}
P1	as cast	2.0×10^{-2}	1.4×10^{-3}	2.3×10^{-2}	−3	7×10^4
P1	annealed[c]	2.4×10^{-2}	1.1×10^{-3}	3.4×10^{-2}	−3	7×10^4
P2	as cast	1.8×10^{-2}	3.1×10^{-3}	2.1×10^{-2}	−8	2×10^5
P2	annealed[d]	4.7×10^{-1}	7.4×10^{-2}	5.4×10^{-1}	−14	5×10^5
P3	as cast	9.3×10^{-3}	1.9×10^{-3}	1.2×10^{-2}	−11	2×10^4
P3	annealed[d]	8.2×10^{-2}	2.7×10^{-3}	8.4×10^{-2}	−5	3×10^4

[a]Average mobility. [b]Maximum mobility. [c]Annealed at 150 °C for 30 min. [d]Annealed at 200 °C for 30 min.

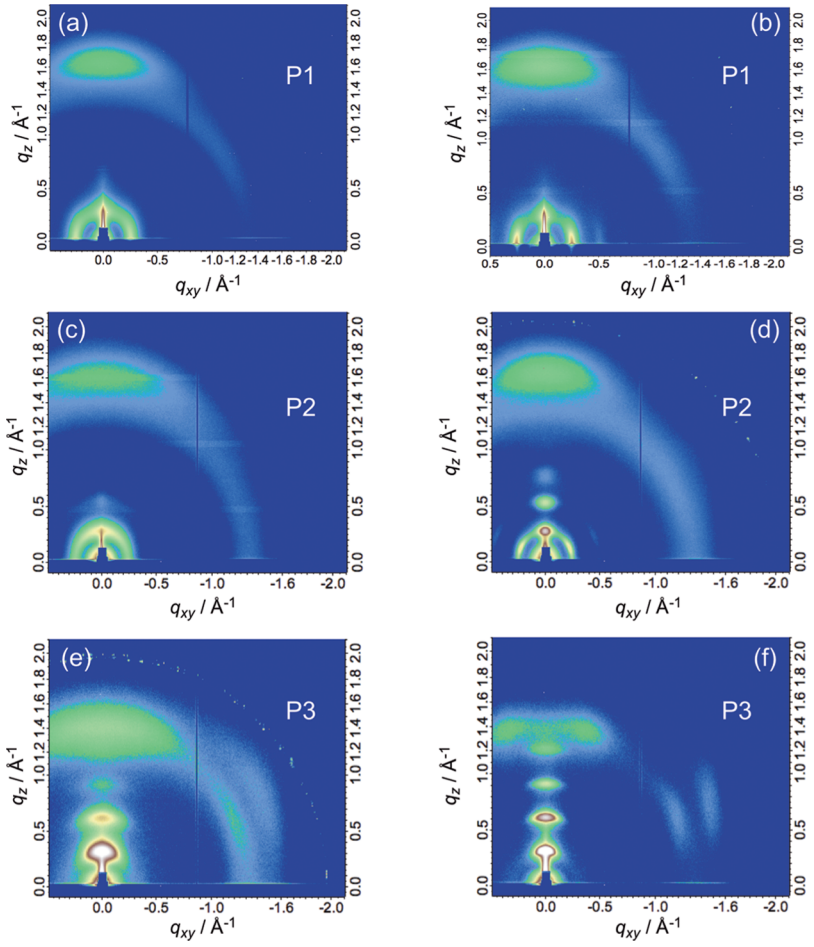

Figure 7. GIWAXS patterns of as cast (a, c, e) and annealed thin films (b, d, f) of **P1−P3**.

DOI: 10.1021/jacs.7b04031
J. Am. Chem. Soc. XXXX, XXX, XXX−XXX

nm. The thin film annealed at 150 °C shows a similar face-on scattering pattern with a new set of diffraction peaks at a *d* spacing of 1.3 nm, which is half that of the (001) peaks, clearly suggesting that these are second-order (002) peaks due to improved in-plane order. The enhanced order in the out-of-plane direction, however, contributes marginally to the in-plane charge transfer, corroborating with the comparable device performances of **P1** thin films with or without thermal treatment. The as-cast thin films of **P2** and **P3** display lamellar structures as indicated by the out-of-plane (n00) peaks. A strong (010) peak is also observed, suggesting the coexistence of both edge-on and face-on crystallites. Upon annealing to 200 °C, the crystallinity of the thin films is greatly enhanced, as indicated by the more confined angular distribution of the peaks and the appearance of higher order out-of-plane diffraction peaks. Additional diffraction peaks with a *d* spacing of 4.3 Å in **P3** suggest that the side chains become more ordered after annealing. The thermally enhanced out-of-plane order in **P2** and **P3** corroborates well with the enhanced charge carrier mobilities. Atomic force microscopic (AFM) images of the annealed polymer films revealed (Figure S5) the formation of fiberlike intercalating networks. The film roughness increases from **P1** (1.12 nm) to **P2** (1.63 nm) to **P3** (4.61 nm), which correlates with the increasing tendency of aggregation when more thiophene units are incorporated in the repeating unit. The larger roughness observed in **P3** may explain its relatively lower mobility than that of **P2** despite its more pronounced lamellar crystallity. Because modification of the polymers by altering the side chain structures is an effective way to enhance molecular order and packing within the thin film,[31] more efficient carrier transport may be realized in AQM-based materials with further side chain engineering.

CONCLUSIONS

In summary, we report the synthesis of an unprecedented stable *p*-azaquinomethane derivative following a succinct two-step synthetic protocol, which involves a Knoevenagel condensation with subsequent alkylation starting from the readily available diketopiperidine derivative. As revealed by single-crystal X-ray structures, the thiophene-flanked *p*-AQMs feature a coplanar structure and rigid conformation with reduced rotational freedom due to intramolecular S···N interactions. Through copolymerization with different oligothiophenes, we have demonstrated that the *p*-AQM is compatible with cross-coupling conditions and can be used to produce a variety of conjugated polymers with tunable band gaps. The *p*-quinoidal structure is directly incorporated in the polymer main chain as part of the resonating structure, which effectively lowers the polymer's band gap via minimization of bond-length alternation. The unique structural features of *p*-AQMs lead to reversed band gap engineering in conjugated polymers that is distinct from the established principles of conventional donor−acceptor polymers and has been further verified by theoretical modeling. Furthermore, GIWAXS studies reveal that these *p*-AQM-containing polymers form highly crystalline structures in the thin film, which are attributable to the compact and planar main chain conformation, reinforced by intramolecular S···N interactions. As a result, the polymers behave as promising hole transporting materials with high charge carrier mobilities reaching 0.54 $cm^2 V^{-1} s^{-1}$. The concise synthetic protocol may stimulate the design and synthesis of new quinoidal building blocks, such as the *o*-AQM homologues. The unique structural and electronic properties of *p*-AQMs render them appealing π-building blocks for next-generation high-performance electronic materials. The photovoltaic performance of such materials is currently under evaluation and will be reported in due course.

ASSOCIATED CONTENT

Supporting Information

The Supporting Information is available free of charge on the ACS Publications website at DOI: 10.1021/jacs.7b04031.

Experimental details for synthesis of monomers and polymers, NMR spectra for intermediates and monomers; CV curves of polymers and small molecules; AFM images for neat annealed polymer films; chemical and X-ray structures of small molecules; calculated frontier orbitals and energies of small molecules; and GPC distribution plots of polymers (PDF)

Crystallographic data for compound **3a** (CIF)

Crystallographic data for compound **4** (CIF)

Crystallographic data for compound **7** (CIF)

AUTHOR INFORMATION

Corresponding Authors

*yliu@lbl.gov

*psjwchen@scut.edu.cn

*bhe@lbl.gov

ORCID

Xuncheng Liu: 0000-0001-5693-6826

Bo He: 0000-0003-1444-4625

Yi Liu: 0000-0002-3954-6102

Author Contributions

#X.L. and B.H. contributed equally to this work.

Notes

The authors declare no competing financial interest.

ACKNOWLEDGMENTS

This work was performed at the Molecular Foundry as a user project and partly supported by the Self-Assembly of Organic/Inorganic Nanocomposite Materials program (B.H., J.K., M.K., L.W., and Y.L.). The X-ray experiments were conducted at the Advanced Light Source (ALS), Lawrence Berkeley National Laboratory, and this work was supported by the Office of Science, Office of Basic Energy Sciences, of the U.S. Department of Energy under Contract No. DE-AC02-05CH11231. X.L. acknowledges support from the China Scholarship Council.

REFERENCES

(1) (a) Zeng, Z.; Wu, J. *Chem. Rec.* **2015**, *15*, 322−328. (b) Sun, Z.; Zeng, Z.; Wu, J. *Acc. Chem. Res.* **2014**, *47*, 2582−2591.

(2) Junkers, T.; Vandenbergh, J.; Adriaensens, P.; Lutsen, L.; Vanderzande, D. *Polym. Chem.* **2012**, *3*, 275−285.

(3) (a) Casado, J.; Ponce Ortiz, R.; Lopez Navarrete, J. T. *Chem. Soc. Rev.* **2012**, *41*, 5672−5686. (b) Sun, Z.; Ye, Q.; Chi, C.; Wu, J. *Chem. Soc. Rev.* **2012**, *41*, 7857−7889. (c) Burrezo, P. M.; Zafra, J. L.; López Navarrete, J. T.; Casado, J. *Angew. Chem., Int. Ed.* **2017**, *56*, 2250−2259. (d) Zeng, Z.; Ishida, M.; Zafra, J. L.; Zhu, X.; Sung, Y. M.; Bao, N.; Webster, R. D.; Lee, B. S.; Li, R.-W.; Zeng, W. *J. Am. Chem. Soc.* **2013**, *135*, 6363−6371. (e) Zeng, Z.; Lee, S.; Son, M.; Fukuda, K.; Burrezo, P. M.; Zhu, X.; Qi, Q.; Li, R.-W.; Navarrete, J. T. L. p.; Ding, J. *J. Am. Chem. Soc.* **2015**, *137*, 8572−8583.

(4) Dou, L.; Liu, Y.; Hong, Z.; Li, G.; Yang, Y. *Chem. Rev.* **2015**, *115*, 12633−12665.

(5) Müllen, K.; Pisula, W. *J. Am. Chem. Soc.* **2015**, *137*, 9503−9505.

(6) (a) van Mullekom, H. A. M.; Vekemans, J. A. J. M.; Havinga, E. E.; Meijer, E. W. *Mater. Sci. Eng., R* **2001**, *32*, 1−40. (b) Brédas, J. *J. Chem. Phys.* **1985**, *82*, 3808−3811.

DOI: 10.1021/jacs.7b04031
J. Am. Chem. Soc. XXXX, XXX, XXX−XXX

(7) (a) Beaujuge, P. M.; Fréchet, J. M. J. *J. Am. Chem. Soc.* **2011**, *133*, 20009−20029. (b) Zhang, Z. G.; Wang, J. *J. Mater. Chem.* **2012**, *22*, 4178−4187.
(8) (a) Wudl, F.; Kobayashi, M.; Heeger, A. J. *J. Org. Chem.* **1984**, *49*, 3382−3384. (b) Brédas, J.; Heeger, A.; Wudl, F. *J. Chem. Phys.* **1986**, *85*, 4673−4678.
(9) Kürti, J.; Surján, P.; Kertesz, M. *J. Am. Chem. Soc.* **1991**, *113*, 9865−9867.
(10) (a) Nayak, K.; Marynick, D. S. *Macromolecules* **1990**, *23*, 2237−2245. (b) Chao, C.-Y.; Chao, C.-H.; Chen, L.-P.; Hung, Y.-C.; Lin, S.-T.; Su, W.-F.; Lin, C.-F. *J. Mater. Chem.* **2012**, *22*, 7331−7341. (c) Cheng, K. F.; Liu, C. L.; Chen, W. C. *J. Polym. Sci., Part A: Polym. Chem.* **2007**, *45*, 5872−5883. (d) Kitamura, C.; Tanaka, S.; Yamashita, Y. *Chem. Mater.* **1996**, *8*, 570−578.
(11) Zhang, H.; Tieke, B. *Polym. Chem.* **2014**, *5*, 6391−6406.
(12) (a) Cui, W.; Yuen, J.; Wudl, F. *Macromolecules* **2011**, *44*, 7869−7873. (b) Cui, W.; Wudl, F. *Macromolecules* **2013**, *46*, 7232−7238. (c) Rumer, J. W.; Rossbauer, S.; Planells, M.; Watkins, S. E.; Anthopoulos, T. D.; McCulloch, I. *J. Mater. Chem. C* **2014**, *2*, 8822−8828.
(13) Kawabata, K.; Saito, M.; Osaka, I.; Takimiya, K. *J. Am. Chem. Soc.* **2016**, *138*, 7725−7732.
(14) Deng, Y.; Sun, B.; He, Y.; Quinn, J.; Guo, C.; Li, Y. *Angew. Chem., Int. Ed.* **2016**, *55*, 3459−3462.
(15) Borthwick, A. D. *Chem. Rev.* **2012**, *112*, 3641−3716.
(16) Gallina, C.; Liberatori, A. *Tetrahedron* **1974**, *30*, 667−673.
(17) The doubly O-alkylated product has been mentioned only once in the literature as a byproduct, see: Ando, S.; Grote, A. L.; Koide, K. *J. Org. Chem.* **2011**, *76*, 1155−1158.
(18) (a) He, B.; Pun, A. B.; Klivansky, L. M.; McGough, A. M.; Ye, Y.; Zhu, J.; Guo, J.; Teat, S. J.; Liu, Y. *Chem. Mater.* **2014**, *26*, 3920−3927. (b) Kroon, R.; Diaz de Zerio Mendaza, A.; Himmelberger, S.; Bergqvist, J.; Bäcke, O.; Faria, G. C.; Gao, F.; Obaid, A.; Zhuang, W.; Gedefaw, D.; Olsson, E.; Inganäs, O.; Salleo, A.; Müller, C.; Andersson, M. R. *J. Am. Chem. Soc.* **2014**, *136*, 11578−11581.
(19) (a) Lin, S.; Wrobleski, S. T.; Hynes, J., Jr; Pitt, S.; Zhang, R.; Fan, Y.; Doweyko, A. M.; Kish, K. F.; Sack, J. S.; Malley, M. F.; Kiefer, S. E.; Newitt, J. A.; McKinnon, M.; Trzaskos, J.; Barrish, J. C.; Dodd, J. H.; Schieven, G. L.; Leftheris, K. *Bioorg. Med. Chem. Lett.* **2010**, *20*, 5864−5868. (b) Conboy, G.; Spencer, H. J.; Angioni, E.; Kanibolotsky, A. L.; Findlay, N. J.; Coles, S. J.; Wilson, C.; Pitak, M. B.; Risko, C.; Coropceanu, V.; Bredas, J.-L.; Skabara, P. J. *Mater. Horiz.* **2016**, *3*, 333−339.
(20) (a) Krüger, H.; Janietz, S.; Sainova, D.; Dobreva, D.; Koch, N.; Vollmer, A. *Adv. Funct. Mater.* **2007**, *17*, 3715−3723. (b) Ahmed, E.; Ren, G.; Kim, F. S.; Hollenbeck, E. C.; Jenekhe, S. A. *Chem. Mater.* **2011**, *23*, 4563−4577.
(21) Xiao, P.; Hong, W.; Li, Y.; Dumur, F.; Graff, B.; Fouassier, J. P.; Gigmes, D.; Lalevée, J. *Polym. Chem.* **2014**, *5*, 2293−2300.
(22) (a) Stalder, R.; Mei, J.; Graham, K. R.; Estrada, L. A.; Reynolds, J. R. *Chem. Mater.* **2014**, *26*, 664−678. (b) Elsawy, W.; Lee, C.-L.; Cho, S.; Oh, S.-H.; Moon, S.-H.; Elbarbary, A.; Lee, J.-S. *Phys. Chem. Chem. Phys.* **2013**, *15*, 15193−15203.
(23) He, B.; Pun, A. B.; Zherebetskyy, D.; Liu, Y.; Liu, F.; Klivansky, L. M.; McGough, A. M.; Zhang, B. A.; Lo, K.; Russell, T. P.; Wang, L.; Liu, Y. *J. Am. Chem. Soc.* **2014**, *136*, 15093−15101.
(24) Wang, X.; Wang, K.; Wang, M. *Polym. Chem.* **2015**, *6*, 1846−1855.
(25) (a) Szumilo, M. M.; Gann, E. H.; McNeill, C. R.; Lemaur, V.; Oliver, Y.; Thomsen, L.; Vaynzof, Y.; Sommer, M.; Sirringhaus, H. *Chem. Mater.* **2014**, *26*, 6796−6804. (b) Durban, M. M.; Kazarinoff, P. D.; Luscombe, C. K. *Macromolecules* **2010**, *43*, 6348−6352. (c) Guo, X.; Watson, M. D. *Org. Lett.* **2008**, *10*, 5333−5336.
(26) Ma, Z.; Sun, W.; Himmelberger, S.; Vandewal, K.; Tang, Z.; Bergqvist, J.; Salleo, A.; Andreasen, J. W.; Inganäs, O.; Andersson, M. R. *Energy Environ. Sci.* **2014**, *7*, 361−369.
(27) (a) Liu, X.; Cai, P.; Chen, Z.; Zhang, L.; Zhang, X.; Sun, J.; Wang, H.; Chen, J.; Peng, J.; Chen, H. *Polymer* **2014**, *55*, 1707−1715. (b) Bin, H.; Gao, L.; Zhang, Z.-G.; Yang, Y.; Zhang, Y.; Zhang, C.; Chen, S.; Xue, L.; Yang, C.; Xiao, M.; Li, Y. *Nat. Commun.* **2016**, *7*, 13651. (c) Bin, H.; Zhang, Z.-G.; Gao, L.; Chen, S.; Zhong, L.; Xue, L.; Yang, C.; Li, Y. *J. Am. Chem. Soc.* **2016**, *138*, 4657−4664.
(28) Kresse, G.; Furthmüller, J. *Phys. Rev. B: Condens. Matter Mater. Phys.* **1996**, *54*, 11169−11186.
(29) Blöchl, P. E. *Phys. Rev. B: Condens. Matter Mater. Phys.* **1994**, *50*, 17953−17979.
(30) (a) Becke, A. D. *J. Chem. Phys.* **1993**, *98*, 5648−5652. (b) Stephens, P. J.; Devlin, F. J.; Chabalowski, C. F.; Frisch, M. J. *J. Phys. Chem.* **1994**, *98*, 11623−11627.
(31) (a) Mei, J.; Bao, Z. *Chem. Mater.* **2014**, *26*, 604−615. (b) Fang, L.; Zhou, Y.; Yao, Y.-X.; Diao, Y.; Lee, W.-Y.; Appleton, A. L.; Allen, R.; Reinspach, J.; Mannsfeld, S. C. B.; Bao, Z. *Chem. Mater.* **2013**, *25*, 4874−4880. (c) Lei, T.; Wang, J.-Y.; Pei, J. *Chem. Mater.* **2014**, *26*, 594−603. (d) Lee, J.; Han, A. R.; Kim, J.; Kim, Y.; Oh, J. H.; Yang, C. *J. Am. Chem. Soc.* **2012**, *134*, 20713−20721.

DOI: 10.1021/jacs.7b04031
J. Am. Chem. Soc. XXXX, XXX, XXX−XXX